batteries

MDPI

Article

The Impact of an Overlaid Ripple Current on Battery Aging: The Development of the SiCWell Dataset

Erik Goldammer [1,*], Marius Gentejohann [2], Michael Schlüter [2], Daniel Weber [3], Wolfgang Wondrak [4], Sibylle Dieckerhoff [2], Clemens Gühmann [3] and Julia Kowal [1]

1 Chair of Electrical Energy Storage Technology (EET), Institute of Energy and Automation, Technische Universität Berlin, Einsteinufer 11, D-10587 Berlin, Germany; julia.kowal@tu-berlin.de
2 Chair of Power Electronics (PE), Institute of Energy and Automation, Technische Universität Berlin, Einsteinufer 19, D-10587 Berlin, Germany; m.gentejohann@tu-berlin.de (M.G.); m.schlueter@tu-berlin.de (M.S.); sibylle.dieckerhoff@tu-berlin.de (S.D.)
3 Chair of Electronic Measurement and Diagnostic Technology (MDT), Institute of Energy and Automation, Technische Universität Berlin, Einsteinufer 17, D-10587 Berlin, Germany; d.weber.1@tu-berlin.de (D.W.); clemens.guehmann@tu-berlin.de (C.G.)
4 Mercedes-Benz AG (MBAG), Research & Development, Hanns Klemm Str. 45, D-71034 Boeblingen, Germany; wolfgang.wondrak@daimler.com
* Correspondence: goldammer@tu-berlin.de

Abstract: Fast-switching semiconductors induce ripple currents on the high-voltage DC bus in the electric vehicle (EV). This paper describes the methods used in the project SiCWell and a new approach to investigate the influence of these overlaid ripples on the battery in EVs. The ripple current generated by the main inverter is demonstrated with a measurement obtained from an electric vehicle. A simulation model is presented which is based on an artificial reference DC bus, according to ISO 21498-2, and uses driving cycles in order to obtain current profiles relevant for battery cycling. A prototype of a battery cycling tester capable of high frequency and precise ripple current generation was developed and is used to cycle cells with superimposed ripple currents within an aging study. To investigate the impact of the frequency and the amplitude of the currents on the battery's lifetime, these ripple parameters are varied between different test series. Cell parameters such as impedance and capacity are regularly characterized and the aging of the cells is compared to standard DC cycled reference cells. The aging study includes a total of 60 automotive-sized pouch cells. The evaluation of ripple currents and their impact on the battery can improve the state-of-health diagnosis and remaining-useful life prognosis. For the development and validation of such methods, the cycled cells are monitored with a measurement system that regularly measures current and voltage with a sampling rate of 2 MHz. The resulting dataset is suitable for the design of future ripple current aging studies as well as for the development and validation of aging models and methods for battery diagnosis.

Keywords: battery aging; ripple current; lithium-ion batteries (LIBs); current harmonics; neural network; electric vehicle; dataset

Citation: Goldammer, E.; Gentejohann, M.; Schlüter, M.; Weber, D.; Wondrak, W.; Dieckerhoff, S.; Gühmann, C.; Kowal, J. The Impact of an Overlaid Ripple Current on Battery Aging: The Development of the SiCWell Dataset. *Batteries* **2022**, *8*, 11. https://doi.org/10.3390/batteries8020011

Academic Editor: Matthieu Dubarry

Received: 8 December 2021
Accepted: 27 January 2022
Published: 31 January 2022

1. Introduction

Figure 1 gives an overview about the structure and the general procedure within the scope of the investigation.

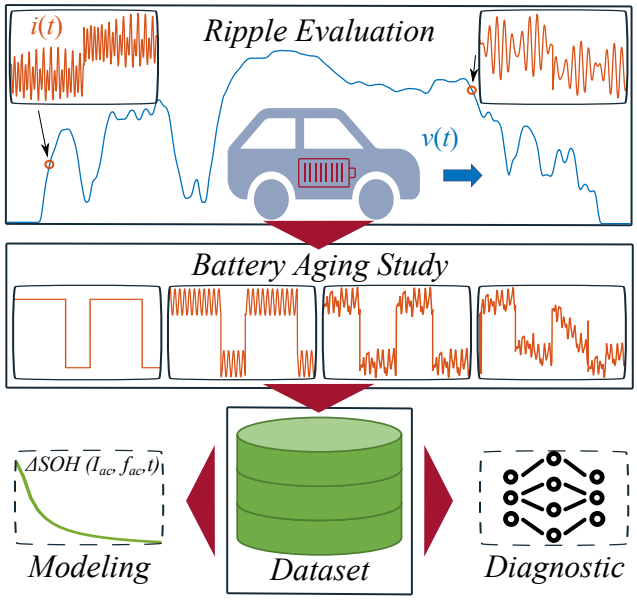

Figure 1. Visual abstract: Structure and method for investigating the influence of ripple currents and development of a corresponding dataset within the SiCWell project [1].

The main traction inverter of an electric vehicle is the electric component with the highest power and highest energy throughput permanently connected to the HV battery and therefore considered the dominant source for the ripple current. This ripple current, generated by the main inverter and its effect on the battery lifetime, is the main contribution of this paper. As shown in Figure 2 on the left, measured in an electric vehicle with a battery capacity of 32 kW h, the voltage ripple has an amplitude up to 10 V and the ripple current exceeds a peak to peak value of 60 A [2]. In the frequency domain, the location and amplitude of the different spectral components (c.f. Figure 2) depend mainly on torque, speed, modulation scheme, switching frequency, dead time, DC link, and DC bus impedance. For transients, more parameters like the control frequency and method become relevant. How the ripple current for the battery cycling is defined and the analysis of the ripple-dependent cell aging are described in detail and discussed in Section 3. Figure 2 was recorded from an electric vehicle [2] under full torque with a speed of approximately 30 km h^{-1} at the terminal of the main inverter using high bandwidth sensors together with a precise oscilloscope on proving ground. These measurements from a real electric vehicle strongly indicate that the ripple current should be considered, i.e., for the battery lifetime, as it exceeds a peak to peak value of 60 A.

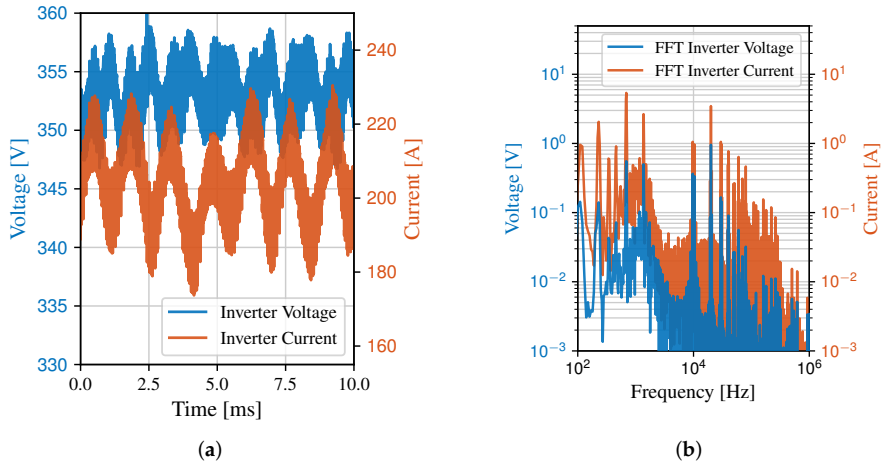

(**a**) (**b**)

Figure 2. DC voltage and current of the main inverter in time (**a**) and frequency domain (**b**).

Due to the increase in the effective current and the associated increase in power loss and temperature, ripple currents are suspected of harming cell performance and lifetime [3,4]. Therefore, the influence of alternating and ripple currents on the degradation of LIBs (lithium-ion batteries) has been investigated in recent years [5–9]. However, these long-term studies conclude different concerning the influence of the ripples. While some studies describe a shortening of the lifetime due to, e.g., local warming, formation of temperature gradients [5,6] or an increased RMS [3], no increase of the aging rate was found in [7–10]. In [11,12], even an increased performance of the examined cells was found for a charge or discharge with superimposed alternating currents (AC).

One reason for the different results could be the large number of adjustable ripple parameters, e.g., waveform, frequency, amplitude, RMS, and peak to peak value. In addition, the examined value ranges of the ripple parameters differ depending on the application and situation under consideration, in some cases by orders of magnitude. In [13], for example, the ripple induced by the grid was considered, and accordingly, the influence of superimposed AC with twice the fundamental frequency (f_g) (120 Hz) was investigated. In [5,6], on the other hand, ripples with frequencies >10 kHz, which are caused by switching processes of the power electronics, were also taken into account.

The large number of ripple parameters and their high bandwidth require a high level of testing effort, even for application-specific investigations into the influence of the ripple current. In addition, commercially available battery testers do not allow a targeted superimposition of a freely adjustable ripple current. Therefore the circuits for the long-term tests must be individually designed and built, as in [5,8,10,11,14].

Besides its effect on the life time of the battery cells, the ripple current has potential benefits for the state of health diagnosis of the battery. The voltage response of the battery cells to the high frequent stimulations of the ripple current contains information of the cell's impedance spectrum, which changes with the aging process. Inspired by the non-linear impedance spectroscopy, machine learning-based methods can be used to estimate the capacity, internal resistance, and impedance spectrum through virtual tests using the ripple current and voltage measured during the daily usage of the battery [15].

The present work aims to create a battery dataset that enables researchers to analyse the influence of ripple currents and develop battery diagnostic methods in a realistic environment. The acquisition of the data and the structure of the dataset are described in this work (see Figure 1). No raw data has yet been published for the studies mentioned, and the authors are also not aware of any sources that provide similar datasets from studies on the long-term exposure of LIBs to ripple currents.

2. Theory

2.1. Ripple Current

Due to the switching nature of power electronic circuits, the DC current is not just changing its DC value because of different operation points; it is always overlaid with an AC ripple. The ripple is generated by the semiconductor switching when converting the DC voltage of the battery to AC with variable frequency and amplitude for the motors or to DC with a different voltage level (e.g., 400 V to 12 V). Although every power electronic circuit has a DC capacitor and additional filters to reduce the disturbances generated during switching operation, this current and voltage ripple should not be neglected while developing the DC bus of an electric vehicle. As investigated in this paper, they affect the aging of the battery cells and can be used as sensor signals to examine the state of charge (SoC) or state of health (SoH) of the battery.

Especially, the topology and switching frequency (f_s) have a strong impact on the ripple current. The current spectrum of an on-board charger is completely different from the spectrum of an electric heater. Only if the topology, switching frequency, and pulse pattern are the same, the generated ripple spectrum of two inverters are similar, which normally is the case for the main traction inverter. Most traction inverters are 2-level 3-phase voltage source inverters with a switching frequency of 10 kHz and a space vector modulation

scheme. In [16], it is shown for steady-state that the DC link current harmonics can be analytically calculated dependent on the above-mentioned parameters. In the SiCWell project [17], special attention has been paid to the switching frequency components of the ripple current because the use of wide-bandgap semiconductors (e.g., silicon carbide) enables an increase of the switching frequencies, which would lead to a shift of the frequency components. The major harmonics in the current spectrum depending on the switching (f_s) and fundamental (f_g) frequency are located at: $f_s \pm 3f_g$; $f_s \pm 6f_g$; $2f_s$; $4f_s$; $2f_s \pm 6f_g$; $3f_g$. The amplitudes strongly depend on the operation point.

2.2. Long-Term Aging Study

The investigation of factors influencing the lifetime of LIBs and the modeling of aging is mainly based on cell aging studies. In such studies, several test series are usually started, between which individual influencing factors are varied. In this way, the long-term influence of the factors on cell parameters, which serve as quality features, is determined. Quality features for batteries of BEVs can be, e.g., capacity, internal resistance, or impedance since these parameters are decisive for the vehicle's available range and performance.

A distinction is made between cyclic (charging and discharging of the cells) and calendar aging tests (storage of the cells). In calendar tests, the influences of temperature and SoC are mainly examined, and the cells remain current-free. On the other hand, cyclic aging tests are performed to evaluate the influence of temperature, DC current, cycle depth (Δ DoD), and the average SoC.

The influence of superimposed AC or ripple currents, on the other hand, has hardly been investigated so far, although a large number of possible investigations are associated with it. Among other parameters, frequency, current amplitude, waveform, edge steepness, etc., can be varied. Figure 3 schematically shows the interaction of adjustable and non-adjustable influencing factors and the quality features in the context of long-term tests on batteries.

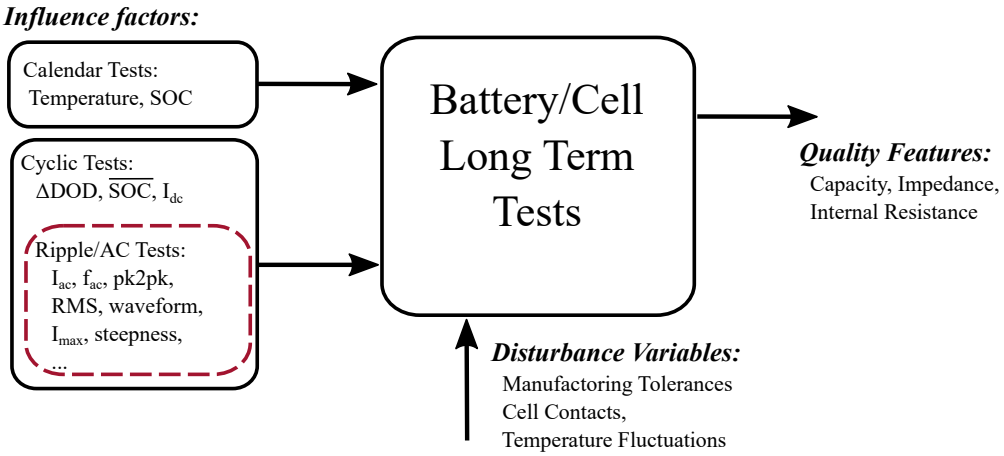

Figure 3. Schematic representation of the system limits and interactions in context of long term tests on batteries. Adjustable and non-adjustable input parameters and battery quality features are shown.

3. Experimental Design

3.1. Modeling of the Ripple Current

The ripple current overlaid to the DC current depends on many different parameters: the battery voltage, the torque and speed demand, the switching and fundamental frequency of the inverter, the DC link, and DC bus impedance—to mention the most important ones. The electrical model shown in Figure 4 considers all these parameters to derive the DC bus ripple current.

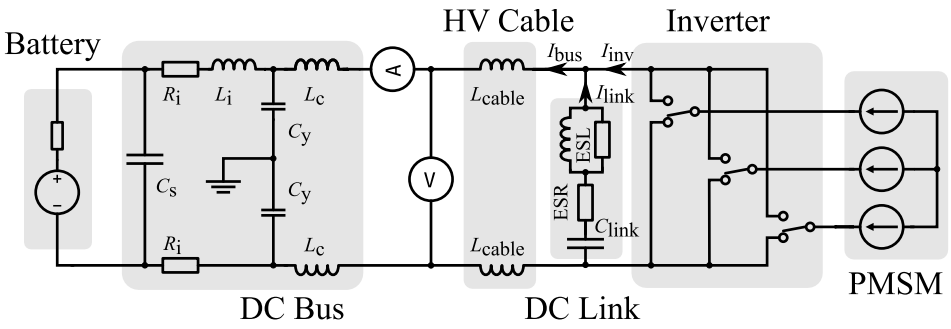

Figure 4. Electric simulation model of the drive train.

The electrical model simulates the resulting currents and voltages in the high voltage DC bus for a given speed and torque. The model follows the architecture proposed in [18] by using a generalized model of the DC bus. The artificial network given in the international standard ISO 21498-2 [19] represents the high voltage battery and defines the parameters of the DC Bus (c.f. Figure 4: R_i, L_i, L_c, C_s, C_y). The HV cable is modeled with an inductance of $L_{cable} = 200$ nH and the DC Link has a capacity of 600 µF, an equivalent series resistances (ESR) of 3 mΩ and an equivalent series inductance of 15 nH. The inverter uses the space vector pulse with modulation (SVPWM) and the operation points are calculated from the torque and speed considering the maximum torque per amp (MTPA) and for higher speeds using field-weakening. More details can be found in [18]. For the drive cycle, c.f. Section 3.2.4, the torque and speed is calculated for every second of the cycle considering parameters like mass of the vehicle, rolling resistance, drag coefficient, front surface and wheel radius. The model does not consider transients and the focus is put on the switching frequency and multiples of the switching frequency. The current obtained on the terminal of the artificial network has to be divided through the number of parallel cell strings (here 2) to obtain the cell current. Considering the above-mentioned limitations the simulation result is a realistic current profile as it could be measured in an EV.

3.2. Long-Term Aging Study

To generate a dataset on the influence of ripple currents, which can be used to parameterize, train, and validate models, lithium-ion pouch cells with a nominal capacity of 50 A h were cycled with pure DC current, DC current with superimposed AC signals, and realistic ripple currents. The active material of the cell's cathode is lithium–manganese–cobalt–oxide (NMC) and that of the anode is graphite. In addition, calendar aging tests were carried out with the same cell type. The various long-term tests are explained in more detail in this chapter.

3.2.1. Sinusoidal and DC Reference Tests

To enable a comprehensive description of the ripple influence and keep the number of necessary test series for this investigation low—despite the high number of ripple parameters—the ripple current was considered in the frequency domain.

Any signal—here, the ripple current—can be reconstructed from the superposition of several sinusoidal oscillations with defined frequencies and amplitudes. The Discrete Fourier Transformation (DFT) is being used to determine the frequency spectrum. Assuming that the effects of the individual frequency components on the cell are additive and time-invariant, it is sufficient to investigate the influence of pure sinusoidal oscillations with amplitudes and frequencies represented in the ripple spectrum (hereinafter referred to as sinusoidal tests). Thus, the possible influencing factors to be varied within the aging study are reduced to amplitude and frequency. Checkups are carried out during the aging study at certain intervals to determine the SoH of the examined cells non-invasively. If the influence of amplitude and frequency on the cell and the SoH is known and the assumptions made are correct, the lifetime can be predicted for any ripple current composed

of the frequency components within the ranges of values investigated. Figure 5 shows schematically the approach chosen to reduce the experimental effort.

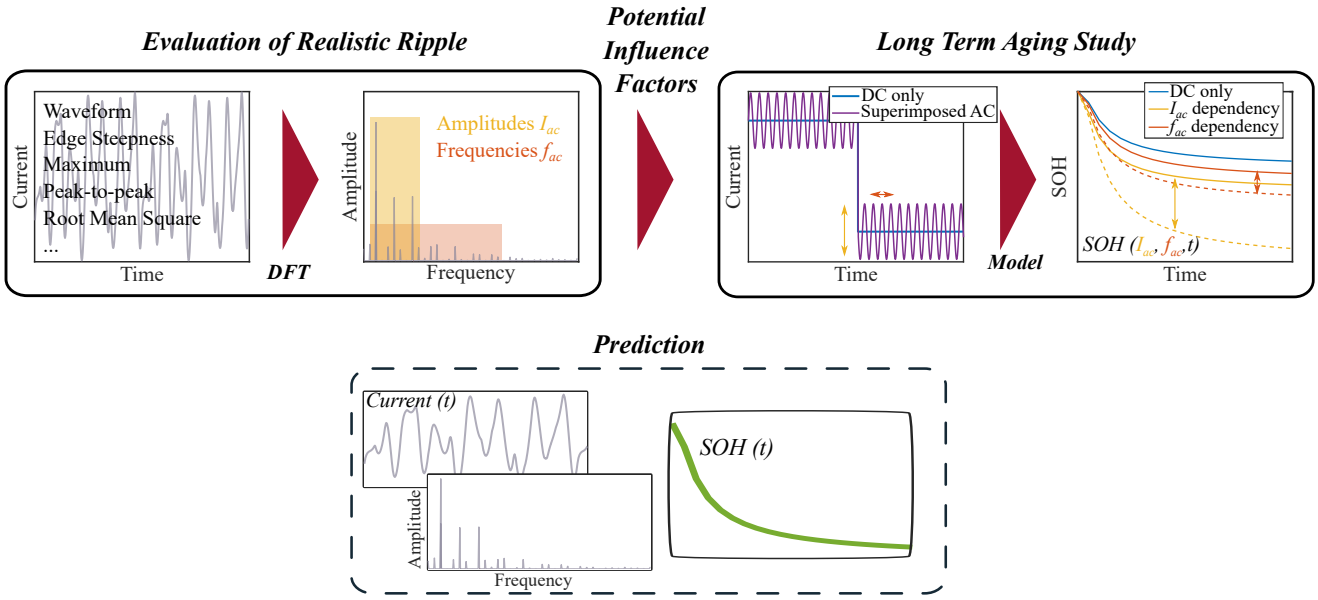

Figure 5. DFT Approach: The frequency domain allows a description of the ripple current based on the parameters frequency and amplitude alone. In an aging study, several test series are started, between which these two potential influencing factors are varied. During the aging tests, checkups are repeatedly performed to determine the SoH of the examined cells as a function of the set frequency and amplitude as well as over time. If the influence of both quantities is known and assuming that the effects of the individual frequency components on the cell are additive and time-invariant, the influence of arbitrary ripple currents can be predicted.

The measurements and simulations of the high-voltage DC bus reveal notable frequency components of the ripple current at single and multiples of the switching frequency. Therefore, 10 kHz (equal to the typical switching frequency of the main inverter) to 40 kHz was chosen as the frequency range to be investigated. For some frequency components, amplitudes up to 10 A could be detected. In view of a possible future reduction of the DC link capacitance for a reduction of space/weight/cost, amplitudes up to 25 A are considered in the investigation. For both amplitude and frequency, test series are started with three different values of each of these factors to be able to derive non-linear dependencies and linear ones. As a reference test, a test series is also started in which no alternating current is superimposed. In Table 1, the set up experimental matrix is shown. In order to estimate the influence of disturbance variables such as manufacturing tolerances, three cells are used per test series for the cyclic aging tests (including the ripple test later on described in this chapter). The cells cycled for the sinusoidal tests are designated (as in the dataset) AC01-AC18. The cells that are cycled with a DC current only are designated as DC01-03.

Table 1. Test matrix of sinusoidal tests.

Frequency \ Amplitude	6.25 A	12.5 A	25 A	0 A
10 kHz	AC07-09	AC01-03	AC04-06	DC01-03
20 kHz		AC13-15		
40 kHz	AC16-18	AC10-12		

Factors influencing the battery beyond the ripple current have already been extensively investigated in other studies. Figure 3 shows known influencing factors such as temperature and SoC. These factors are kept constant for each series of sinusoidal tests in order to be able to investigate the influence of frequency and amplitude specifically. The values were chosen so that the cell is subjected to a realistic load, and the influence by these non-ripple factors can be considered low to moderate, according to existing studies. Thus, the ripple-induced aging of the studied cell is less overshadowed by other aging effects. Table 2 shows the set values of the factors.

Table 2. Standard settings of cyclic aging tests.

DC charge current ($I_{dc,ch}$)	0.75 C
DC discharge current ($I_{dc,dis}$)	1.6 C
End of charge voltage ($V_{ch,end}$)	4.0 V
Cycle depth (ΔDoD)	≈30%
Average SoC ($\overline{SoC}$)	≈60%
Ambient temperature (T_{amb})	25 °C

3.2.2. Calendar Tests

In addition to cyclic aging tests, calendar aging tests are also performed at various state of charges (SoCs) and ambient temperatures. The superimposed AC currents during the sinusoidal tests could result in an additional increase of the cell temperature compared to the ambient temperature due to increased RMS values. The results from the calendar aging tests allow separate consideration of the effect of any temperature rise and the direct effects of ripple current on the cell. In Table 3, the experimental matrix of the calendar aging tests is given. Two cells are used for each test series of the calendar aging tests. The calendar aged cells are designated (as in the dataset) Ka01-Ka12.

Table 3. Test matrix of calendar tests.

Temperature \ **SoC**	**20%**	**45%**	**60%**	**80%**
35 °C		Ka03/04		Ka01/02
45 °C	Ka07/08	Ka09/10	Ka11/12	Ka05/06

3.2.3. Artificial Ripple Tests

For the validation of the selected approach, a test series is also carried out in which four sinusoidal oscillations with different amplitudes $I_{ac,1...4}$ and frequencies $f_{ac,1...4}$ are superimposed on the DC current instead of one (hereinafter referred to as the ripple test I).

Only if the effects of the individual sinusoidal oscillations on the aging of the cells are time-invariant and additive as assumed, the results of the sinusoidal tests can be used to predict the aging behavior in the ripple test I with the chosen approach (compare Figure 5). Thus, it is checked whether the results from the sinusoidal tests are transferable and allow an estimation of the effect of a realistic ripple or independent modeling of their influence since realistic ripples contain multiple frequency components.

The frequencies and amplitudes of the four superimposed components are selected based on the simulated ripple currents (see Table 4) at characteristic operating points (OPs). A total of three OPs are taken into account. The four main frequency components of one OP are superimposed on the DC current for one DC cycle. During the entire following DC cycle, the main frequency components of another OP are superimposed. After three cycles, the main components of all three OPs have been superimposed, and the overall sequence is repeated. The considered OPs are not only characteristic but also chosen to cover the whole frequency range studied in the sinusoidal tests. Table 4 gives an overview of the

superimposed AC components during ripple cycling. The other influencing factors were again selected according to Table 2.

Table 4. Superimposed AC at ripple test.

Operating Point (OP) \ AC	$I_{ac,1}/f_{ac,1}$	$I_{ac,2}/f_{ac,2}$	$I_{ac,3}/f_{ac,3}$	$I_{ac,4}/f_{ac,4}$
Ripple OP1	11.28 A/9 kHz	7.02 A/11 kHz	2.62 A/10 kHz	2.53 A/20 kHz
Ripple OP2	12.01 A/19 kHz	9.00 A/21 kHz	2.57 A/40 kHz	2.23 A/16 kHz
Ripple OP3	7.20 A/40 kHz	4.77 A/20 kHz	-	-

3.2.4. Realistic Ripple Tests

The experiments developed to this point allow for qualitative and quantitative analyses of the influence of ripple currents on the battery lifetime. More representative current profiles are required to develop, validate, and compare battery diagnosis methods in the context of daily driving an electric vehicle. In the process of developing a data-based diagnostic model, the parameters of a model are fitted to a training dataset, and the resulting model is validated on a validation dataset. The training and validation data have to come from different distributions to evaluate the generalizability and detect overfitting. In the case of the battery dataset, this means that two different current profiles for cycling the batteries are required so that the model cannot just memorize the current sequence. To achieve these current profiles, two reference driving profiles commonly used to evaluate the range and emission of vehicles are simulated with a vehicle model. The chosen driving profiles are the Worldwide harmonized light-duty test cycle (WLTC) [20] and the urban dynamometer driving schedule (UDDS) [21] because they both have a broad range of vehicle speeds and accelerations. The speed demands of the former driving cycle are scaled which results in higher speeds and higher accelerations in a more realistic scenario. In the following, it is referred to as scaled WLTC (sWLTC).

For a virtual EV to be simulated, the mechanical data of a Mercedes Benz E-Class are used which are stored in the dataset. Based on its parameters, a mechanical model calculates the demanded force for every second of the driving cycles and derives the electrical motor's rotational units, speed, and torque. These operation points are used in the electrical model (c.f. Section 3.1) to derive the set points for the inverter and the electrical motor considering their control scheme. Then, the model is simulated for each of the operation points in steady state.

The simulated battery current is post-processed. Ref. [18] shows various criteria to evaluate the ripple current, i.e., the increased power dissipation due to the ripple. Here, the simulated battery current is used to define a profile for battery test cycling. With the discrete Fourier transformation, the current is calculated in the frequency domain. At each operation point, a specific current spectrum is obtained. The four frequency components with the highest amplitude and the DC component are picked for each point of the cycle. By storing the DC component as well as amplitude, phase, and frequency of the four components, the current profile is compressed. The battery cycler controls the five components individually in the frequency domain. By this scheme, the system can handle very high frequencies (up to 40 kHz) with feedback control of the measured battery currents.

Different charging and discharging strategies than in the other tests are required to achieve a more realistic cycling of the battery cells. To simulate the irregular charging behavior of daily driving, the SoC limits for charging and discharging change every cycle. To reduce the overfitting of data-based models, the discharging starts at different points of the current profiles.

3.2.5. Checkups

Checkups are performed at regular intervals to determine the quality features of the cell. In the case of calendar aging tests, the checkup is performed after a specified time interval, and in the case of cyclic aging tests, after a specified number of cycles. Since formation processes (e.g., solid electrolyte interface (SEI) formation) may not be fully completed at the beginning of the aging tests, an increased rate of change of some cell parameters is to be expected [7]. Since previous studies have found an influence of ripple current on forming processes [7] and SEI [5,6], the checkups will initially be performed at shorter intervals (in terms of time and the number of cycles) to track these changes.

Each checkup includes a capacitance measurement and a total of four impedance measurements and pulse tests at 20%, 40%, 60% and 80% SoC, respectively, (here called regular checkup). The flow of a regular checkup and the resulting current and voltage curve is shown in Figure 6.

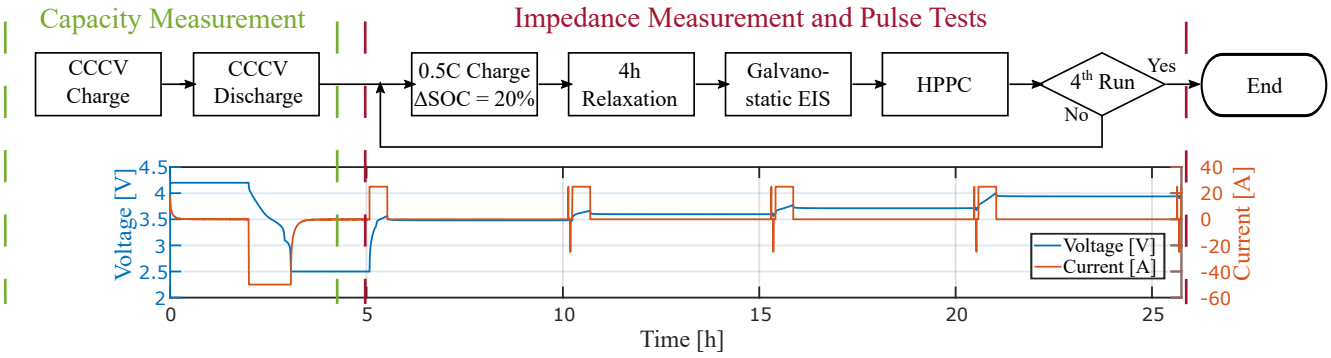

Figure 6. Regular Checkup: Procedure to characterize the capacity of the cell as well as impedance and pulse behavior at different SoC levels.

The capacity corresponds to the amount of charge removed/measured during the constant-current constant-voltage (CCCV) discharge. Due to the CV phases, a superimposed influence of the cell impedance on the measured capacity is largely eliminated. The steps shown for impedance measurement and pulse tests are repeated four times so that impedance spectra and pulse data are available for different SoC levels. First, the cells are charged with a constant-current (CC) charge until the SoC has increased by 20%. Before the impedance measurement by means of electrochemical impedance spectroscopy (EIS), the cells are relaxed for 4 h. Following the EIS, a hybrid pulse power characterization (HPPC) test is performed. This includes a 10 s charge and discharge pulse. Before and after each pulse, the cell is relaxed for 3 min to minimize the influence of the previous excitation on the measurement and to record the relaxation behavior. The regular checkup is completed after the fourth run of the described procedure, i.e., after EIS and HPPC at 80% SoC.

The metadata of the pulse tests (pulse resistances), as well as the impedance and capacitance measurement, are available in the provided dataset in the checkups folder. In addition, the raw data are included in the dataset. This includes the current, voltage, and temperature curves during the CCCV discharge for the capacity determination, as well as current and voltage curves during the HPPC tests (separated by discharge and charge pulse). In order to be able to derive the dynamics of slow processes with large time constants, current and voltage during charging by 20% SoC including the subsequent four-hour relaxation are also given.

The regular checkup is followed by the measurement of the open-circuit voltage (OCV). After an initial checkup, recording is performed less frequently than the regular checkup because the measurement of OCV takes more time and further differential voltage and incremental capacity analysis (DVA and ICA) are subject to greater inaccuracies (compared to capacity and impedance analyses) [22]. Therefore, a meaningful evaluation/analysis of the OCV requires major changes in the aging state of the cell.

An incremental measurement method was used to determine the OCV since a better approximation to the actual OCV curve is achieved for the same amount of time as when a low constant current is applied [23]. In addition, high-resolution pulse measurement data is available over the complete SoC range, which can be used for further analyses [24].

Figure 7 shows the sequence of the incremental OCV (iOCV) measurement in the flow chart, as well as the resulting voltage and current curves for the individual steps.

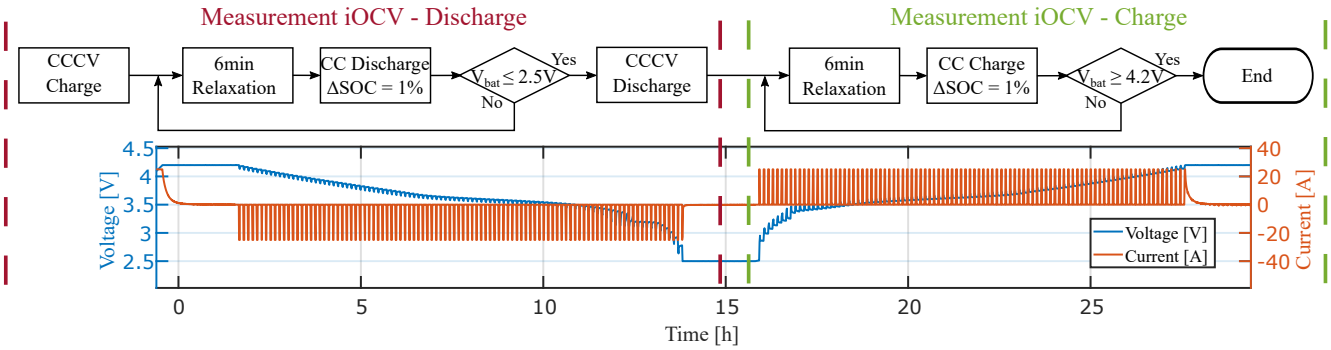

Figure 7. Incremental OCV measurement: Procedure to record the OCV curve in discharge and charge direction of the investigated cells and simultaneously obtain high-resolution pulse data over the complete SoC range.

The OCV measurement points are plotted over removed charge quantity as described in [25]. The metadata (OCV via removed charge) can be found in the dataset. In addition, for user-specific evaluations, the raw data of the pulses taking place every 1% SoC as part of the OCV measurement are also supplied.

The iOCV method is also used with 5% SoC steps but 4 h relaxation for an even better approximation to the real OCV (at worse resolution). However, due to the high time requirement, the iOCV with 4 h relaxation is only performed during the initial and the final checkup following the iOCV measurement with 6 min relaxation.

4. Experimental Setup

To realize the ambient temperature of the experimental matrices and to ensure a low fluctuation, all cells are housed in MK240 temperature chambers from Binder with appropriately set internal temperatures. The recording of the impedance spectra during a checkup is done with the Potentiostat 5000E from Gamry. The links to the datasheets for the climatic chambers, the potentiostat, and the test equipment described below (Solfas and ARBIN battery tester) can be found in the appendix.

4.1. Test Bench DC Reference and Calendar Tests

The test series with pure DC load (reference test) is performed with the ARBIN LBT22013. One channel of the battery tester can realize an output voltage of 0–25 V and a current of up to ±100 A. The three cells of the DC test series are connected in series to form stacks of three and connected to a channel to load all three cells with the same current profile during cycling. Current profile and cycle settings are selected according to the values given in Table 2.

For the calendar tests, the cells are brought to a voltage corresponding to the SoC to be set according to the test matrix Table 3 and then stored in a climatic chamber at the temperature intended for the test series.

For the checkups, all test series cells are connected individually to one channel of the ARBIN (cyclic and calendar aged). The checkups are always performed at 25 °C. For this reason, the calendar-aged cells are also placed in a temperature chamber with an internal temperature of 25 °C during a checkup and stored there for 4 h without load at 25 °C in order to reduce any temperature gradients.

Surface temperature, voltage, and current of the cells are measured and stored at a minimum sampling rate of 0.1 Hz during cycling and checkups.

4.2. Test Bench Sinusoidal/Ripple Tests

The test setup of the ripple and sinusoidal tests is visualized in Figure 8. It is composed of a newly developed battery tester, which can generate ripple currents, an impedance measurement device for checkups, an external measurement system for high resolution current and voltage measurements, and a computer that controls the hardware and processes the measurements.

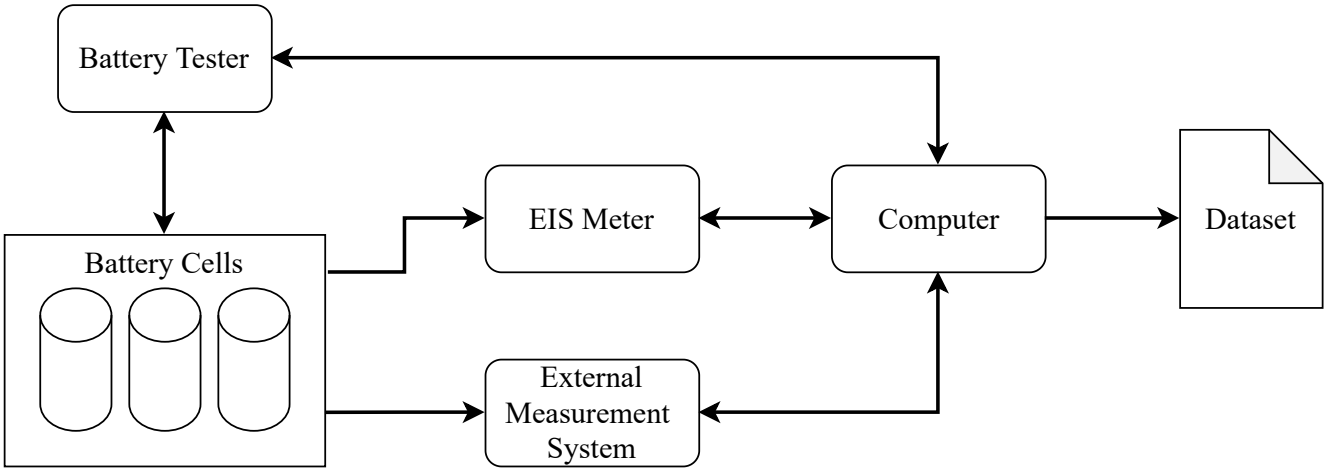

Figure 8. The test setup of the ripple tests consists of a computer that controls the battery tester, which cycles the battery cells, an impedance measurement device for checkups, and an external measurement system, which measures current and voltage with high sampling rates.

The battery tester, developed in cooperation with Solfas GmbH, was set up for cyclization with superimposed AC components. In addition to the standard functions of a commercially available battery tester, it meets the following requirements concerning overlaying AC components:

- Superposition of 1–4 sinusoidal oscillations to the applied DC current with freely adjustable amplitudes and frequencies
  - Amplitudes: 0–25 A, 10 mA resolution
  - Frequency range: 1–50 kHz; 1 kHz resolution

Since the developed system (in contrast to the conventional cyclers) can automatically switch a channel to the individual cells of a stack or the complete stack, it is not necessary to manually reconnect the cells for the checkup. Here, too, the checkup (as well as the cyclization) takes place in a climatic chamber at 25 °C.

Similar to the reference and calendar tests, the surface temperature, voltage, and current of the cells are measured during cycling and checkups with a sampling rate between 0.1 and 100 Hz.

To enable more detailed analysis methods of the AC components, a separate measurement system has been integrated that has a higher sampling rate and resolution. It comprises a fast and accurate analog-digital-converter (ADC) and a multiplexer that connects the ADC to every battery channel. To enable the analysis of low amplitude signals with frequencies of several kilohertz, a high signal-to-noise ratio, resolution, and sampling rate is required. Because of that, the ADC has a sampling rate of 2 MS/s, 18-bit resolution, and measures the three voltages and the current of a channel simultaneously and differentially. All cables used for measurements are shielded and have minimized lengths below one meter.

5. Results

The present work aims to create a dataset that contains all information required to evaluate ripple currents and their influence on batteries in a battery electric vehicle. The resulting dataset contains the vehicle and drive train parameters used to simulate the current profiles in this work and a high and low-resolution version of the current profiles themselves. For evaluating the battery aging, the periodic cell checkups of the calendar, dc, sinusoidal, artificial ripple, and realistic ripple tests are made available. For developing diagnosis and prognosis battery models, the current, voltage, and temperature data are made available in the time domain for the whole duration of the sinusoidal, artificial ripple, and realistic ripple tests.

These components can be grouped by their potential applications, as illustrated in Figure 9. The vehicle model and current profiles can be used for further studies, the raw cycle measurements for the development of diagnostic and prognostic models, and the checkups of the battery cycles for modeling the aging process.

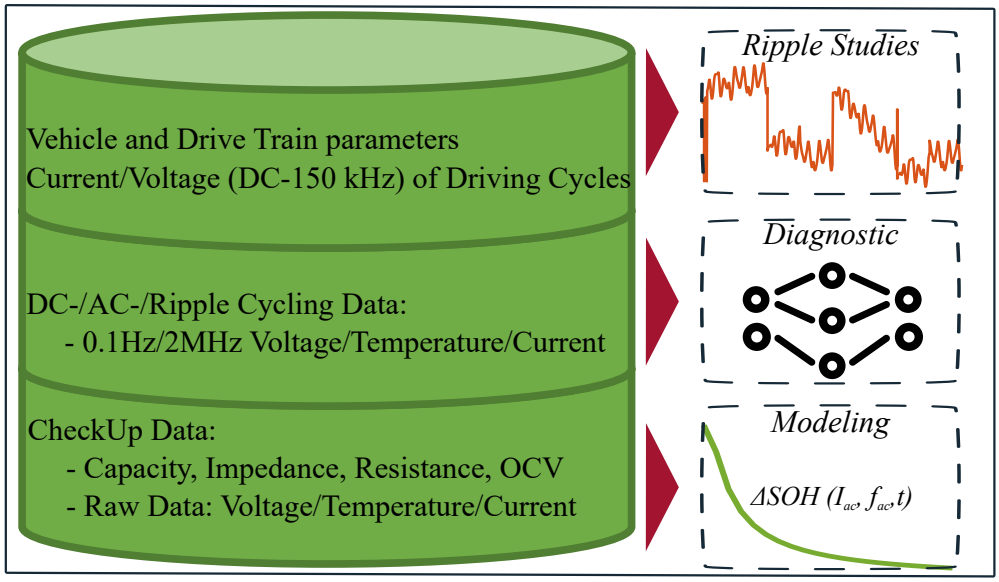

Figure 9. The structure and main components and their potential applications of the present work's dataset.

Figure 10 consists of three spectrograms that show the frequency components of the ripple current during the 1800 s of the scaled WLTC. The frequency components obtained from the simulation model (c.f. Sections 3.1 and 3.2.4) are presented in Figure 10a. Significant frequency components are found at the double switching frequency (20 kHz) and at sidebands of the single switching frequency. The ripple current compressed to its four highest components is plotted in Figure 10b, while Figure 10c shows the ripple current measured at the battery tester. Comparing the three heatmaps, it is seen that the same frequency components are obtained for every second of the cycle, which leads to the conclusion that the characteristic of the cycle is preserved when the cycle is compressed. The simulated, compressed, and measured cycles are stored in the dataset for both driving cycles (sWLTC and UDDS).

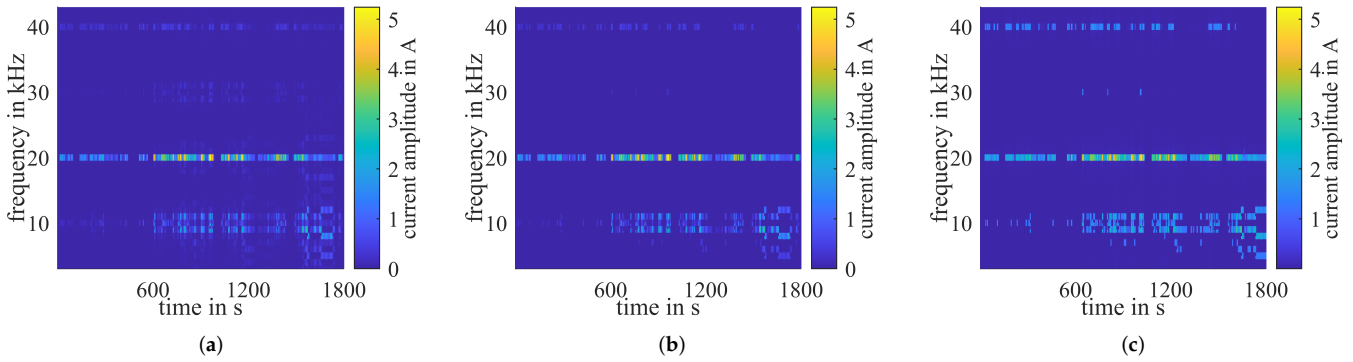

Figure 10. Frequency components of the ripple current over the driving cycle obtained by simulation (**a**,**b**) and measurement at the battery tester (**c**). (**a**) Simulated sWLTC; (**b**) compressed sWLTC; (**c**) measured sWLTC at battery tester.

Figure 11 shows the capacity curve measured for a test series of sinusoidal/ripple tests and DC reference scenario (mean value per test series). The Figure shows that the superimposed AC components have a negative influence, which leads to a significant reduction in the available capacity. If 45 A h is defined as the end of life (EoL) of the cells (approx. 80% of the initially measured capacity), the results shown in Figure 11 indicate a significant reduction in the lifetime of the cells when AC or ripple currents are superimposed. Depending on the superimposed sinusoidal or ripple current, the ampere-hour throughput until the EoL of the cells was reached reduced between 13 up to 45% (45% for ripples containing realistic frequency components for specific operating points—see Section 3.2.3). Thus, the shown results support the thesis that realistic ripples caused by the switching processes of semiconductors contribute to an additional and non-negligible aging of the cells in an EV. Therefore, according to the results of this study, the influence of ripple currents should be taken into account in the design of the high-voltage DC bus. In turn, this also requires corresponding models about the influence.

Furthermore, a dependence on the amplitude and frequency of the superimposed oscillations can be seen in Figure 11. An increase in capacity loss can be observed both for higher amplitudes and when the frequency is doubled from 10 to 20 kHz. Therefore, the data are suitable for modeling the influence of ripple on battery life as a function of frequency and amplitude (see Figure 5).

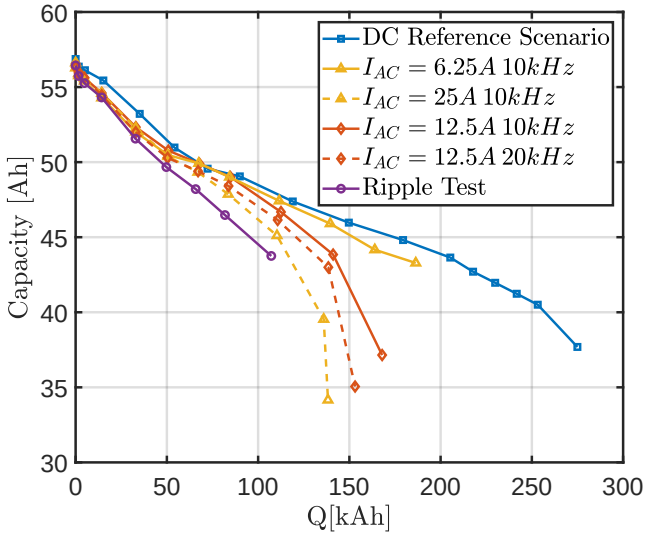

Figure 11. Capacity change during cyclic aging of cells of different test series.

6. Conclusions

In order to derive a realistic current profile for battery cycling, this study uses a simulation model which determines the DC current and its superimposed ripple depending on the operation point. From a measurement of a real vehicle, it is seen that significant components are found at multiples of the switching frequencies or their sidebands. These components are also derived from the simulation model. Considering a virtual EV, the current profile is calculated for two driving cycles used for the battery cycling tests.

A new approach is described for investigating the effects of the identified ripple currents, which helps to reduce the testing effort for future investigations. The approach allows a reduction of the number of influencing factors to be investigated to amplitude and frequency. In addition, the value ranges of these ripple parameters were narrowed down by specifically evaluating the application-specific ripple current, i.e., the ripple in the high-voltage DC bus. Thus, the number of required test series is reduced. The reduction in testing effort is particularly important because aging studies concerning the ripple current are also connected with the construction of own test benches.

The aging study conducted investigates the ripple currents induced by the traction inverter and the switching semiconductors in the high-voltage DC bus and the associated influence on the battery in a EV. In addition to previous studies, ripple currents are considered for all operation points that occur during realistic driving cycles. The results of the extensive aging study expands the comparatively small data basis on the ripple impact and can be used to determine the reason for the different results of previous ripple studies and to verify the results shown there.

The practical application of the methods developed in this work resulted in the SiCWell dataset, which is helpful for various applications in battery research. The cycling data of the battery are well suited for developing and validating state-of-health diagnosis methods in a realistic environment. The realistic ripple tests of the dataset contain the current profiles of two driving cycles applied to multiple battery cells. This results in a benchmark for a broad range of battery diagnosis methods. Furthermore, the raw and metadata of the dataset can be used to derive aging models for the influence of AC currents. Aging models that describe the influence of the ripple current on the battery's lifetime offer the possibility of deriving optimizations of the hardware and software of the high-voltage DC bus concerning the ripple current based on simulations. For example, the large and expensive DC link capacitor, can be scaled down to fit the aging target of the battery. Another example is the switching frequency of the inverter, which can be chosen corresponding to the ripple currents the battery is less sensitive to.

The dataset is publicly available at [1].

Author Contributions: Conceptualization, E.G., M.G., M.S. and D.W.; methodology, E.G., M.G., M.S. and D.W.; software, E.G., M.G., M.S. and D.W.; validation, E.G., M.G., M.S. and D.W.; formal analysis, E.G., M.G., M.S. and D.W.; investigation, E.G., M.G., M.S. and D.W.; data curation, E.G., M.G., M.S. and D.W.; writing—original draft preparation, E.G., M.G., M.S. and D.W.; writing—review and editing, S.D., C.G., J.K., E.G., M.G., M.S. and D.W.; visualization, E.G., M.G., M.S. and D.W.; supervision, S.D., C.G., J.K. and W.W.; project administration, S.D., C.G., J.K. and W.W.; funding acquisition, S.D., C.G., J.K. and W.W. All authors have read and agreed to the published version of the manuscript.

Funding: This research was funded by Bundesministerium für Bildung und Forschung (BMBF) under grant number 16EMO0262 (SiCWell).

Data Availability Statement: Publicly available datasets were analyzed in this study. This data can be found here: [1,2].

Acknowledgments: The authors would like to thank the German Federal Ministry of Education and Research (BMBF) for funding this project, as well as Clemens Wache and their team from Solfas GmbH, in particular Thomas Leist, for developing and supplying the battery tester and for their valuable support during commissioning.

Conflicts of Interest: The authors declare no conflict of interest. The funders had no role in the design of the study; in the collection, analyses, or interpretation of data; in the writing of the manuscript, or in the decision to publish the results.

Abbreviations

The following abbreviations are used in this manuscript:

AC	Alternating current
CC	Constant-current
CCCV	Constant-current-constant-voltage
DC	Direct current
DFT	Discrete Fourier Transformation
DOAJ	Directory of open access journals
DoD	Depth of discharge
DVA	Differential voltage analysis
EET	Electrical Energy Storage Technology
EIS	Electrochemical impedance spectroscopy
EV	Electric vehicle
ICA	Incremental capacity analysis
HPPC	Hybrid pulse power characterization
LIBs	Lithium-ion batteries
MDPI	Multidisciplinary Digital Publishing Institute
MDT	Electronic Measurement and Diagnostic Technology
OCV	Open-circuit voltage
OP	Operating point
PE	Power Electronics
SEI	Solid electrolyte interface
SoC	State of charge
SoH	State of health
UDDS	Urban Dynamometer Driving Schedule
WLTC	Worldwide harmonized Light-duty Test Cycle

References

1. Weber, D.; Gentejohann, M.; Goldammer, E.; Schlüter, M.; Dieckerhoff, S.; Gühmann, C.; Kowal, J. The SiCWell Dataset. *IEEE DataPort* **2021**. [CrossRef]
2. Schlüter, M.; Gentejohann, M.; Dieckerhoff, S. High Bandwidth On-Board DC Voltage and Current Measurements of the Main Inverter of an Electric Vehicle. *IEEE DataPort* **2021**. [CrossRef]
3. Juang, L.W.; Kollmeyer, P.J.; Anders, A.E.; Jahns, T.M.; Lorenz, R.D.; Gao, D. Investigation of the influence of superimposed AC current on lithium-ion battery aging using statistical design of experiments. *J. Energy Storage* **2017**, *11*, 93–103. [CrossRef]
4. Savoye, F.; Venet, P.; Pelissier, S.; Millet, M.; Groot, J. Impact of periodic current pulses on Li-ion batteries lifetime in vehicular application. *Int. J. Electr. Hybrid Veh.* **2015**, *7*, 323. [CrossRef]
5. Uddin, K.; Moore, A.D.; Barai, A.; Marco, J. The effects of high frequency current ripple on electric vehicle battery performance. *Appl. Energy* **2016**, *178*, 142–154. [CrossRef]
6. Uddin, K.; Somerville, L.; Barai, A.; Lain, M.; Ashwin, T.R.; Jennings, P.; Marco, J. The impact of high-frequency-high-current perturbations on film formation at the negative electrode-electrolyte interface. *Electrochim. Acta* **2017**, *233*, 1–12. [CrossRef]
7. Brand, M.J.; Hofmann, M.H.; Schuster, S.S.; Keil, P.; Jossen, A. The Influence of Current Ripples on the Lifetime of Lithium-Ion Batteries. *IEEE Trans. Veh. Technol.* **2018**, *67*, 10438–10445. [CrossRef]
8. Bessman, A.; Soares, R.; Wallmark, O.; Svens, P.; Lindbergh, G. Aging effects of AC harmonics on lithium-ion cells. *J. Energy Storage* **2019**, *21*, 741–749. [CrossRef]
9. Amamra, S.A.; Tripathy, Y.; Barai, A.; Moore, A.D.; Marco, J. Electric Vehicle Battery Performance Investigation Based on Real World Current Harmonics. *Energies* **2020**, *13*, 489. [CrossRef]
10. Soares, R.; Bessman, A.; Wallmark, O.; Lindbergh, G.; Svens, P. An Experimental Setup with Alternating Current Capability for Evaluating Large Lithium-Ion Battery Cells. *Batteries* **2018**, *4*, 38. [CrossRef]
11. Chen, L.R.; Chen, J.J.; Ho, C.M.; Wu, S.L.; Shieh, D.T. Improvement of Li-ion Battery Discharging Performance by Pulse and Sinusoidal Current Strategies. *IEEE Trans. Ind. Electron.* **2013**, *60*, 5620–5628. [CrossRef]
12. Chen, L.R.; Wu, S.L.; Shieh, D.T.; Chen, T.R. Sinusoidal-Ripple-Current Charging Strategy and Optimal Charging Frequency Study for Li-Ion Batteries. *IEEE Trans. Ind. Electron.* **2013**, *60*, 88–97. [CrossRef]

13. Prasad, R.; Namuduri, C.; Kollmeyer, P. Onboard unidirectional automotive G2V battery charger using sine charging and its effect on li-ion batteries. In Proceedings of the 2015 IEEE Energy Conversion Congress and Exposition (ECCE), Montreal, QC, Canada, 20–24 September 2015; pp. 6299–6305. [CrossRef]
14. Beh, H.Z.Z.; Covic, G.A.; Boys, J.T. Effects of pulse and DC charging on lithium iron phosphate (LiFePO4) batteries. In Proceedings of the 2013 IEEE Energy Conversion Congress and Exposition, Denver, CO, USA, 15–19 September 2013; pp. 315–320. [CrossRef]
15. Klass, V.; Behm, M.; Lindbergh, G. Capturing lithium-ion battery dynamics with support vector machine-based battery model. *J. Power Sources* **2015**, *298*, 92–101. [CrossRef]
16. McGrath, B.P.; Holmes, D.G. A General Analytical Method for Calculating Inverter DC-Link Current Harmonics. *IEEE Trans. Ind. Appl.* **2009**, *45*, 1851–1859. [CrossRef]
17. SiCWell—Einfluss von Siliziumcarbid-Wechselrichtern auf die Lebensdauer von Traktionsbatterien. Available online: https://www.elektronikforschung.de/projekte/sicwell (accessed on 26 January 2022).
18. Gentejohann, M.; Schlüter, M.; Hepp, M.; Dieckerhoff, S. Driving Cycle Analysis of the DC Bus Current Ripple in Electric Vehicles. In Proceedings of the 2021 23rd European Conference on Power Electronics and Applications (EPE'21 ECCE Europe), Virtual Conference, Ghent, Belgium, 6–10 September 2021.
19. ISO 21498-2:2021. *Electrically Propelled Road Vehicles—Electrical Specifications and Tests for Voltage Class B Systems and Components—Part 2: Electrical Tests for components*; ISO: Geneva, Switzerland, 2021.
20. Tutuianu, M.; Bonnel, P.; Ciuffo, B.; Haniu, T.; Ichikawa, N.; Marotta, A.; Pavlovic, J.; Steven, H. Development of the World-wide harmonized Light duty Test Cycle (WLTC) and a possible pathway for its introduction in the European legislation. *Transp. Res. Part Transp. Environ.* **2015**, *40*, 61–75. [CrossRef]
21. Kruse, R.E.; Huls, T.A. Development of the Federal Urban Driving Schedule. In *National Automobile Engineering Meeting*; SAE International: Warrendale, PA, USA, 1973. [CrossRef]
22. Pastor-Fernández, C.; Yu, T.F.; Widanage, W.D.; Marco, J. Critical review of non-invasive diagnosis techniques for quantification of degradation modes in lithium-ion batteries. *Renew. Sustain. Energy Rev.* **2019**, *109*, 138–159. [CrossRef]
23. Petzl, M.; Danzer, M.A. Advancements in OCV Measurement and Analysis for Lithium-Ion Batteries. *IEEE Trans. Energy Convers.* **2013**, *28*, 675–681. [CrossRef]
24. Wildfeuer, L.; Gieler, P.; Karger, A. Combining the Distribution of Relaxation Times from EIS and Time-Domain Data for Parameterizing Equivalent Circuit Models of Lithium-Ion Batteries. *Batteries* **2021**, *7*, 52. [CrossRef]
25. Barai, A.; Widanage, W.D.; Marco, J.; McGordon, A.; Jennings, P. A study of the open circuit voltage characterization technique and hysteresis assessment of lithium-ion cells. *J. Power Sources* **2015**, *295*, 99–107. [CrossRef]